10858 *Biochemistry* **2009,** *48,* 10858–10865
DOI: 10.1021/bi901373e

BIOCHEMISTRY
including biophysical chemistry & molecular biology
*Article*

# Single-Molecule Analysis of the Human Telomerase RNA·Dyskerin Interaction and the Effect of Dyskeratosis Congenita Mutations†

Beth Ashbridge,[‡,⊥] Angel Orte,[‡,⊥,@] Justin A. Yeoman,[‡,⊥,#] Michael Kirwan,[∥] Tom Vulliamy,[∥] Inderjeet Dokal,[∥] David Klenerman,*[,‡,▽] and Shankar Balasubramanian*[,‡,§,▽]

[‡]*University Chemical Laboratories, University of Cambridge, Lensfield Road, Cambridge CB2 1EW, U.K.,* [§]*School of Clinical Medicine, University of Cambridge, Cambridge CB2 0SP, U.K., and* [∥]*Centre for Paediatrics, Institute of Cell and Molecular Science, Barts and The London School of Medicine and Dentistry, Queen Mary, University of London, London E1 2AT, U.K.*
[⊥]*These authors contributed equally to this work.* [@]*Present address: Department of Physical Chemistry, Faculty of Pharmacy, Campus Cartuja, Granada 18071, Spain.* [#]*Present address: National Centre for Biological Sciences, Tata Institute of Fundamental Research, UAS GKVK, Bellary Road, Bangalore 560 065, India.*
[▽]*Joint senior authorship.*

*Received August 7, 2009; Revised Manuscript Received October 1, 2009*

ABSTRACT: It has been proposed that human telomerase RNA (hTR) interacts with dyskerin, prior to assembly of the telomerase holoenzyme. The direct interaction of dyskerin and hTR has not been demonstrated and is an experimentally challenging research problem because of difficulties in expressing and purifying dyskerin in quantities that are useful for biophysical analysis. By orthogonally labeling dyskerin and hTR, we have been able to employ single-molecule two-color coincidence detection (TCCD) to observe directly the formation of a dyskerin·hTR complex. By systematic deletion of hTR subdomains, we have gained insights into the RNA sites required for interaction with dyskerin. We then investigated mutated forms of hTR and dyskerin that are associated with dyskeratosis congenita (DC), on the basis of clinical genetics studies, for their effects on the dyskerin·hTR interaction. Dyskerin mutations associated with X-linked DC resulted in significant impairment of the dyskerin·hTR interaction, whereas mutations in hTR associated with autosomal dominant (AD) DC did not affect the interaction. We propose that disruption of the dyskerin·hTR interaction may contribute to X-linked DC.

Dyskerin is a putative pseudouridine synthase that is expressed constitutively and is required for correct modification of ribosomal and small nuclear RNA precursors (*1*). A complex capable of pseudouridylation is formed by dyskerin and three other proteins, NOP10, NHP2, and GAR1, in association with a specific guide RNA containing the box H/ACA sequence motif (*2*, *3*). The presence of this motif in the 3′ half of the RNA component of human telomerase (hTR)[1] has been proposed to provide a discrete binding site for dyskerin within the telomerase complex (*2*, *4*). hTR provides the template for telomere synthesis by human telomerase reverse transcriptase (hTERT) and acts as a protein-binding scaffold for telomerase holoenzyme assembly (*5*). Recently, the protein dyskerin has been identified as a component of active human telomerase purified from cells (*6*, *7*) in addition to hTERT and hTR. It has been hypothesized that dyskerin is linked in a spatiotemporal manner to the biogenesis of the pre-telomerase RNP (*7*) and/or the stabilization of hTR within the telomerase complex, but there has been no explicit physical evidence of a direct interaction between hTR and dyskerin.

Dyskeratosis congenita (*8*, *9*) is thought to be the first primary telomere maintenance disorder to be identified in humans. It is a premature aging syndrome that can lead to a triad of mucocutaneous features, namely, abnormal skin pigmentation, nail dystrophy, and mucosal leukoplakia (*10*). DC adversely affects highly proliferative tissues, with bone marrow failure being the major cause of death (*11*). Cells from patients with this disease generally display short telomeres, and the lack of efficient telomere maintenance has been attributed to reduced levels of active telomerase enzyme. DC is a genetically diverse condition and arises from three possible inheritance patterns. The most common is the X-linked form, which is associated with mutations in the *DKC1* gene that encodes dyskerin (*12*, *13*). Patients with X-linked DC, mainly young males, go on to develop bone marrow failure before the age of 30 (*14*) and have an increased risk of cancer, which is thought to arise because shortened telomeres promote genomic instability. More recently, an autosomal dominant form of the disease has been characterized, in which patients generally display milder symptoms that present later in life. A major subset of cases, demonstrating a clinically heterogeneous phenotype, are associated with mutations in hTR (*15*).

Physical analysis of the components of the telomerase complex has been hampered by technical challenges because of low natural abundance, poor expression, and inefficient in vitro assembly of the recombinant enzyme. In our hands, human dyskerin has proven to be similarly difficult to express at high levels

†This work was supported by the BBSRC, the Wellcome Trust (Grant 069399/Z/02), and the MRC (Grant G0400534). A.O. thanks the Marie Curie IEF of the sixth EU Framework for financial support.

*To whom correspondence should be addressed. (S. B.) Telephone: +44 (0) 1223 336347. Fax: +44 (0) 1223 336913. E-mail: sb10031@cam.ac.uk. (D.K.) Telephone: +44 (0) 1223 336481. E-mail: dk10012@cam.ac.uk.

[1]Abbreviations: DC, dyskeratosis congenita; AD DC, autosomal dominant dyskeratosis congenita; hTR, human telomerase RNA; hTERT, human telomerase reverse transcriptase; TCCD, two-color coincidence detection; YFP, yellow fluorescent protein; 647N−RNA, RNA molecule conjugated to the maleimide derivative of ATTO-TEC 647N fluorescent dye; PUA, pseudouridine and archaeosine transglycosylase; PCR, polymerase chain reaction; RNP, ribonucleoprotein.

 Published on Web 10/17/2009 

(greater than picomoles) in vitro, which precludes the use of most classical biophysical methods that require at least 1000-fold greater sample quantities for effective analysis. Our single-molecule fluorescence approach two-color coincidence detection (TCCD) can overcome such limitations as it requires a minimal quantity (less than femtomoles) of labeled components. Furthermore, it can be used to characterize a partially purified complex of orthogonally labeled species in the presence of a high background of labeled, unassociated molecules (*16*−*18*). The advantage of TCCD compared to other single-molecule techniques, such as FRET, is that the fluorophore label can be placed at any convenient position on the molecule, and that no prior knowledge of the complex structure is required. Furthermore, the cross-talk between channels is weak, making the method significantly more sensitive to low concentrations of associated molecules.

Herein, we describe the use of single-molecule TCCD to detect and study the dyskerin·hTR complex. In particular, we evaluated the dependence of this protein·RNA interaction on subdomains of hTR and on mutations associated with the rare human disease DC.

## MATERIALS AND METHODS

*Construction of the pET28a-3×FLAG-YFP-DKC1 Plasmid*. The *DKC1* coding sequence had previously been cloned from human cDNA and inserted into the pEF1 plasmid vector (Invitrogen, Paisley, U.K.). The sequence was subsequently amplified by PCR using the forward primer 5′-CTT AGT GCT AGC ATG GCG GAT GCG GAA GTA ATT ATT TTG C-3′, containing the NheI restriction site, and the reverse primer 5′-AGA TCT GAA TTC CTA CTC AGA AAC CAA TTC TAC C-3′, containing the EcoRI restriction site. The *DKC1* PCR product was subjected to double-restriction endonuclease digestion with enzymes NheI and EcoRI and subcloned into a pET28a vector containing the 3×FLAG coding sequence to produce pET28a-3×FLAG-DKC1. The YFP coding sequence was amplified by PCR from plasmid pET28a-3×FLAG-YFP-hTERT using the forward primer 5′-TAT ACA GCT AGC GTG AGC AAG GGC GAG GAG C-3′ and the reverse primer 5′-AGA TCT GCT AGC CTT GTA CAG CTC GTC CAT GCC-3′, both containing the NheI restriction site. The YFP PCR product was subjected to restriction endonuclease digestion with NheI and subcloned into the pET28a-3×FLAG-DKC1 plasmid to produce pET28a-3×FLAG-YFP-DKC1. The final construct was verified by DNA sequencing (Cogenics Lark, Takeley, U.K.).

*Construction of the pIRES2-3×FLAG-YFP-DKC1-EGFP Plasmid*. The pET28a-3×FLAG-YFP-DKC1 plasmid was subjected to double-restriction endonuclease digestion with enzymes BglI and EcoRI, and the insert 3×FLAG-YFP-DKC1 was subjected to gel purification on a preparative agarose gel. The gel-purified DNA fragment was subcloned into the pIRES2-EGFP vector (BD Biosciences, Oxford, U.K.) to produce pIRES2-3×FLAG-YFP-DKC1-EGFP. The final construct was verified by DNA sequencing (Cogenics Lark).

*Functional Analysis of the 3×FLAG-YFP-DKC1 Protein*. HEK 293 cells were seeded at a density of $4 \times 10^5$ cells/well in a six-well plate in DMEM-F12 with 10% fetal calf serum (Lonza, Wokingham, U.K.). After 24 h, cells were cotransfected with 1 mg of pIRES2-EGFP (empty vector) or pIRES2-3×FLAG-YFP-DKC1-EGFP and 1 mg of the anti-dyskerin shRNA SHCLNG-NM_001363, TRCN0000039738 (Sigma-Aldrich, Gillingham, U.K.), using Lipofectamine LTX (Invitrogen) according to the manufacturer's protocol. A knockdown negative control consisted of transfection of 2 mg of pIRES2-EGFP alone. Cells were cultured at 37 °C for 72 h before being harvested by trypsinization. Successfully transfected, GFP-positive cells were selected using a BD FACSAria cell sorter (BD Biosciences) and separated into two aliquots for further analysis.

Telomerase enzyme activity was measured using the telomerase repeat amplification protocol (TRAP) assay (*19*) using the TRAPeze RT Telomerase Detection Kit (Millipore, Watford, U.K.) according to the manufacturer's protocol. Briefly, lysates of 3,000 cells were incubated at 30 °C for 30 min in the presence of a substrate oligonucleotide for the addition of telomeric repeats. The products of this incubation were amplified by real-time quantitative PCR, and the fluorescein-labeled products were detected on an ABI 7500 Real-Time PCR System (Applied Biosystems, Warrington, U.K.).

To determine cellular hTR levels, RNA was prepared from 50,000 cells using the RNeasy Mini Kit (Qiagen, Crawley, U.K.). Random hexamers (Qiagen) and M-MLV reverse transcriptase (Invitrogen) were used to synthesize first-strand cDNA according to the manufacturer's protocol. Absolute RNA expression of the hTR gene and the *ABL1* housekeeping gene was assessed by quantitative real-time PCR on an ABI 7500 Real-Time PCR System (Applied Biosystems) as described previously (*20*). hTR gene transcript levels were normalized to the level of *ABL1* expression to compensate for loading variation.

*Fluorescence Properties of the Two Fluorophores*. YFP has a fluorescence excitation maximum at 514 nm and a fluorescence emission maximum at 527 nm, whereas the red maleimide dye ATTO 647N (ATTO-TEC GmbH, Siegen, Germany) has a fluorescence excitation maximum at 644 nm and a fluorescence emission maximum at 669 nm. A 488 nm laser line was used to selectively excite YFP, whereas a 633 nm laser line was used to selectively excite ATTO 647N.

*Mutagenesis of pET28a-3×FLAG-YFP-DKC1 and pUC18-hTR Plasmids*. pET28a-3×FLAG-YFP-DKC1 plasmid constructs containing one of the dyskeratosis congenita point mutations (C146T, C1058T, or G1205A) and pUC18-hTR plasmid constructs containing one of the dyskeratosis congenita point mutations (G309T, C408G, or G450A) were prepared using the QuikChange II site-directed mutagenesis kit (Stratagene, La Jolla, CA) following the manufacturer's protocol. The PCR primers used are detailed in Table S1 of the Supporting Information. Each of the final constructs was verified by DNA sequencing (Cogenics Lark).

*Preparation of Fluorescently Labeled hTR Fragment Constructs*. DNA templates suitable for runoff in vitro transcription of full-length hTR, hTR(1−354), and hTR(1−208) were generated by restriction endonuclease digestion of plasmid pUC18-hTR with BamHI, StuI, and PpuMI, respectively. The sequence encoding hTR nucleotides 353−451 was amplified by PCR using the forward primer 5′-TAC TGT AAG CTT TAA TAC GAC TCA CTA TAG GCC TTT CAG GCC GCA GGA AG-3′, designed to include the 17-nucleotide T7 promoter and the HindIII restriction site, the reverse primer 5′-TAC TGT GGA TCC GCA TGT GTG AGC CGA GTC CTG G-3′, designed to include the BamHI restriction site, and plasmid pUC18-hTR as a template. The PCR product of nucleotides 353−451 of hTR was subjected to double-restriction endonuclease digestion with enzymes HindIII and BamHI and subcloned

into the pUC18 vector to produce pUC18-hTR(353−451). The final construct was verified by DNA sequencing (Cogenics Lark). A DNA template suitable for runoff in vitro transcription of hTR(353−451) was generated by restriction endonuclease digestion of plasmid pUC18-hTR(353−451) with BamHI. The RNA-$\gamma$-S molecules hTR-$\gamma$-S, hTR(1−354)-$\gamma$-S, hTR(1−208)-$\gamma$-S, and hTR(353−451)-$\gamma$-S, containing a unique sulfur atom modification at the $\gamma$-phosphate of the 5′ end nucleotide, were generated by runoff in vitro transcription using T7 RNA polymerase in the presence of guanosine-5′-*O*-(3-thiotriphosphate), GTP-$\gamma$-S. They were subsequently reacted with the $C_2$ maleimide derivative of ATTO 647N to produce 647N−hTR, 647N−hTR-(1−354), 647N−hTR(1−208), and 647N−hTR(353−451).

*Protein Expression and Reconstitution with Human Telomerase RNA*. Dyskerin, labeled at the N-terminus with yellow fluorescent protein (YFP) and a 3×FLAG tag, was generated by coupled transcription and translation in a rabbit reticulocyte lysate cell-free TNT T7 Quick Coupled Transcription/Translation System (Promega, Southampton, U.K.) in the presence of 647N−hTR to produce YFP−dyskerin·647N−hTR. Briefly, 8 $\mu$g of pET28a-3×FLAG-YFP-DKC1 plasmid, 20 pmol of 647N−hTR, and 4 nmol of methionine were added to 200 $\mu$L of TNT Quick Master Mix. The expression mixture was incubated at 30 °C for 90 min. This type of in vitro expression approach has been frequently used for the assembly of active human telomerase from recombinant hTR and hTERT (*21*).

*Affinity-Based Purification of Dyskerin·hTR RNP*. The YFP−dyskerin·647N−hTR RNP complex formed during coupled in vitro transcription and translation was purified via the integral N-terminal 3×FLAG tag. All steps of the purification were performed at 4 °C. A 1.7 mL microcentrifuge tube was loaded with 50 $\mu$L of anti-FLAG M2 affinity gel suspension (Sigma-Aldrich) and centrifuged at 706*g* for 1 min. The supernatant was removed, and 500 $\mu$L of wash buffer A [25 mM Tris-HCl (pH 7.4), 50 mM KCl, 5 mM $MgCl_2$, 1 mM EDTA, 10% (v/v) glycerol, and 0.1% (v/v) Nonidet P40 Substitute] was added. The tube was inverted by hand 10 times and centrifuged at 706*g* for 1 min, and the supernatant was removed. The gel was washed two additional times according to the same protocol; 500 $\mu$L of blocking buffer A [25 mM Tris-HCl (pH 7.4), 50 mM KCl, 5 mM $MgCl_2$, 1 mM EDTA, 10% (v/v) glycerol, 0.1% (v/v) Nonidet P40 Substitute, 0.5 mg/mL BSA, and 0.1 mg/mL yeast tRNA] was added and the microcentrifuge tube inverted at 12 rpm on a rotator for 30 min. The tube was centrifuged at 706*g* for 1 min, and the supernatant was removed. The gel was blocked a second time for 30 min according to the same protocol. In parallel, after the protein expression and RNP complex reconstitution, 400 $\mu$L of blocking buffer B [25 mM Tris-HCl (pH 7.4), 50 mM KCl, 5 mM $MgCl_2$, 1 mM EDTA, 20% (v/v) glycerol, 0.2% (v/v) Nonidet P40 Substitute, 1 mg/mL BSA, and 0.2 mg/mL yeast tRNA] was added to the expression mixture, the microcentrifuge tube inverted five times, and the blocking mixture centrifuged at 16,708*g* for 20 min. The supernatant was removed from any precipitated material and applied to the blocked anti-FLAG affinity gel. The tube containing the gel was inverted at 12 rpm on a rotator overnight. The following day, the gel was washed six times with 500 $\mu$L of blocking buffer A according to the same protocol used during gel preparation; 150 $\mu$L of elution buffer A [25 mM Tris-HCl (pH 7.4), 50 mM KCl, 5 mM $MgCl_2$, 1 mM EDTA, 10% (v/v) glycerol, 0.1% (v/v) Nonidet P40 Substitute, 0.3 mg/mL 3×FLAG peptide (Sigma-Aldrich), and 0.1 mg/mL BSA] was added to the gel and the tube inverted at 12 rpm on a rotator for 60 min. The tube was centrifuged at 706*g* for 1 min, and the supernatant was removed and divided into 5 × 30 $\mu$L aliquots. The aliquots were snap-frozen and stored at −80 °C.

*Two-Color Coincidence Detection of the Dual-Labeled Dyskerin·hTR Complex*. The purified YFP−dyskerin·647N−hTR sample was subjected to single-molecule TCCD analysis. The apparatus and experimental method have been detailed in previous studies (*16*, *17*, *21*). Experiments were performed on a home-built two-color confocal inverted microscope setup, which incorporated a diode laser (488 nm, model Cyan CDRH, Newport Spectra-Physics, Didcot, U.K.) and a cylindrical helium/neon laser (633 nm, model 25 LHP 151-230, Melles Griot, Cambridge, U.K.). The two Gaussian laser beams were overlapped and directed to the back port of an inverted microscope (model Eclipse TE2000-U, Nikon, Kingston upon Thames, U.K.). The laser beams were focused 6 $\mu$m into the sample solution through a high-numerical aperture oil immersion objective lens (NA 1.40, model Apochromat 60×, Nikon). Fluorescent light emitted by the sample was collected back through the objective lens and directed to a 50 $\mu$m pinhole (Melles Griot). The pinhole rejected out of focus fluorescent and other background light and defined the probe volume within the sample solution from which a fluorescence signal was recorded. The remaining light was separated according to wavelength by a dichroic mirror (model 585DRLP, Omega Optical, Brattleboro, VT) and focused onto two avalanche photodiodes (SPCM AQR-14, Perkin-Elmer Optoelectronics, Cambridge, U.K.). The signal from each avalanche photodiode was processed using a separate multichannel scalar, MCS, card, integrating fluorescence signal in 1 ms time bins. The sample to be analyzed was thawed and immediately diluted on the microscope stage to an approximate dyskerin concentration of 10 pM in dilution buffer [25 mM Tris-HCl (pH 7.4), 50 mM KCl, 5 mM $MgCl_2$, 1 mM EDTA, 20 $\mu$g/mL BSA, and 10 $\mu$g/mL yeast tRNA] in a total volume of 1 mL in a Lab-TeK chambered coverglass (Scientific Laboratory Supplies, Hessle, U.K.). The laser powers were 220 and 60 $\mu$W for 488 and 633 nm excitation, respectively. Data were collected at 20 °C, and fluorescence bursts in both channels were then subjected to background and cross-talk correction, thresholding, and analysis for coincidence.

*Two-Color Coincidence Detection Data Analysis*. The coincidence value or association quotient, $Q$, is defined as the ratio of the rate of significant coincident events, $r_{sig}$, to the sum of the rate of all events in blue and red channels, $r_{blue}$ and $r_{red}$, respectively, with a correction to avoid double counting of coincident events (eq 1).

$$\begin{aligned} Q &= r_{sig}/(r_{blue} + r_{red} - r_{sig}) \\ &= (r_{coin} - r_{exp})/[r_{blue} + r_{red} - (r_{coin} - r_{exp})] \end{aligned} \quad (1)$$

The significant coincident event rate is obtained by subtraction of the expected rate of coincident events due to chance, $r_{exp}$, from the observed rate of coincident events, $r_{coin}$. Coincident events due to chance arise from noninteracting molecules labeled with different fluorophores that happen to be in the confocal excitation volume simultaneously. The expected rate of these events is determined on the basis of probabilistic calculations and described in detail by Orte and co-workers (*17*). In our measurements, between 25 and 50% of the coincident events were due to chance because of the low concentration of fully assembled

complex, but their contribution was effectively removed by desynchronizing in time the traces from the blue versus the red channel, giving rise to only chance coincidence that is subtracted from the total coincidence and the total TCCD histogram (*17*). The association quotient, $Q$, is linearly related to the mole fraction of species containing both fluorescent labels, according to the detection efficiency of the instrument. This was determined by analysis of a model DNA control sample consisting of a duplex in which each strand was labeled with one or other of the red and blue fluorophores and which was taken to be 100% dual-labeled.

Stoichiometric information relating to a coincident species was extracted through analysis of the coincidence histogram. The function $Z = \ln(I_{red}/I_{blue})$ was plotted, where $I_{red}$ and $I_{blue}$ are the intensities of coincident events in the red and blue channels, respectively, after background and cross-talk correction. The resulting frequency distribution was fitted with one or more normal distribution functions. Each function has a peak center, $\langle Z \rangle$, and width, $\sigma$, related to the mean fluorophore brightness values $\langle I_{red} \rangle_f$ and $\langle I_{blue} \rangle_f$ according to eqs 2 and 3.

$$\langle Z \rangle \approx \ln(n\langle I_{red} \rangle_f / m\langle I_{blue} \rangle_f) \quad (2)$$

$$\sigma = (K/n\langle I_{red} \rangle_f + K/m\langle I_{blue} \rangle_f)^{1/2} \quad (3)$$

The inclusion of an extra Gaussian function in the fitting process was justified by a decrease in the fitting parameter $\chi^2$ of >20%, and by F tests.

## RESULTS AND DISCUSSION

To study the interaction between dyskerin and hTR, we labeled each component with fluorophores that could be excited independently. hTR, containing a single 5′-thiophosphate functionality, was generated by in vitro transcription prior to reaction with the maleimide derivative of the fluorophore ATTO 647N (ATTO-TEC GmbH) to produce 647N−hTR, which we have previously demonstrated does not impair telomerase catalytic activity (*21*). Dyskerin was labeled at the N-terminus with yellow fluorescent protein (YFP) and a 3×FLAG tag to produce the YFP−dyskerin protein. To verify that N-terminal modification had not impaired dyskerin function with respect to telomerase, the YFP−dyskerin fusion protein was "knocked-in" to HEK 293 cells by cotransfection of a plasmid encoding the modified dyskerin gene and an anti-"endogenous dyskerin" small hairpin RNA (shRNA) plasmid. The shRNA plasmid was either transfected alone, as a negative control, or co-transfected with the construct pIRES2-3×FLAG-YFP-DKC1-EGFP. The standard markers of normal dyskerin function related to telomerase within the cell, hTR levels and telomerase activity, were recorded. Transfection of HEK 293 cells with the shRNA plasmid alone led to a reduction of hTR levels to 42.2 ± 6.2% and telomerase activity to 15.2 ± 1.0% relative to those of cells transfected with the empty pIRES2-EGFP vector alone (Figure 1A,B). Cotransfection of the shRNA plasmid and the construct pIRES2-3×FLAG-YFP-DKC1-EGFP afforded hTR levels of 86.7 ± 12.0% and a telomerase activity of 58.5 ± 12.6% relative to those of cells transfected with the empty pIRES2-EGFP vector alone. We have therefore shown that N-terminally modified dyskerin rescued the reduction of hTR levels and telomerase enzyme activity seen in shRNA-only transfected cells, confirming that YFP−dyskerin protein supports normal cellular function with respect to the telomerase complex and in particular the accumulation of hTR.

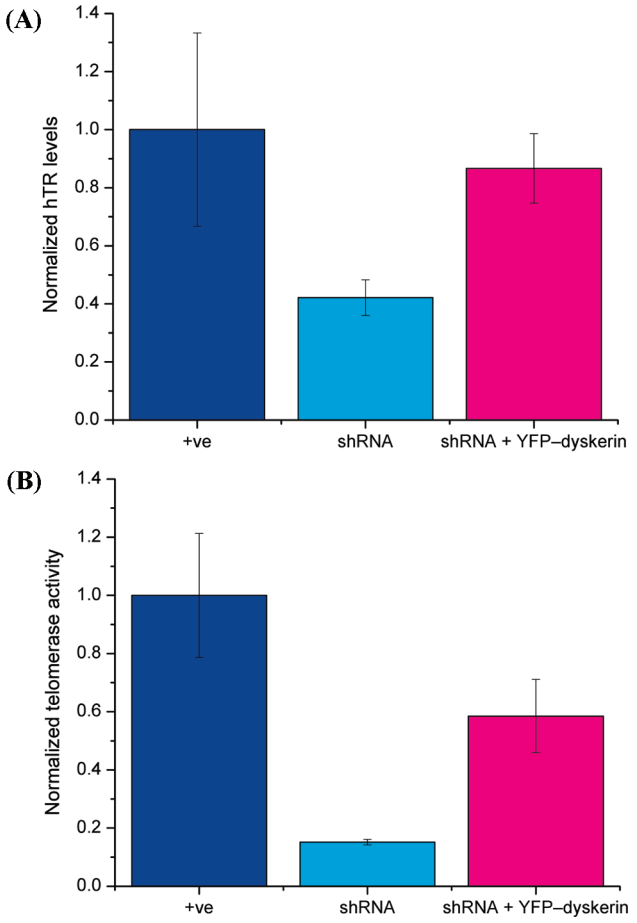


FIGURE 1: Function of N-terminally tagged dyskerin in HEK 293 cells: (A) hTR levels and (B) telomerase activity.

YFP−dyskerin protein was prepared by coupled transcription and translation in a rabbit reticulocyte lysate cell-free system, in the presence of 647N−hTR. Purification of YFP−dyskerin protein and any associated RNA was achieved by immunoprecipitation using an anti-FLAG antibody. Such an in vitro expression−purification approach has been used routinely for the assembly of active human telomerase from recombinant hTR and hTERT (*21*). The purified YFP−dyskerin·647N−hTR sample was subjected to single-molecule TCCD analysis (Figure 2A) at a concentration around 10 pM. We observed a direct interaction between YFP−dyskerin protein (blue) and 647N−hTR (red) by TCCD, by detecting coincident fluorescent bursts in both channels from associated YFP−dyskerin·647N−hTR complexes (Figure 2B). The detected coincidence levels corresponded to 4.8 ± 1.1% of the total labeled molecules present being involved in complexes containing at least one YFP−dyskerin and one 647N−hTR component. A coincidence histogram (Figure 2C) of the data was constructed as a function of $\ln(I_{red}/I_{blue})$, where $I_{red}$ and $I_{blue}$ are the red and blue fluorescence intensities of each coincident event, respectively, to elucidate the stoichiometry of complexes present (*17*, *21*). The normal distribution centered closest to zero corresponds to a complex containing an equal number of YFP−dyskerin and 647N−hTR molecules. More detailed analysis of the intensities of the fluorescent bursts showed that this distribution is mainly (>75%) composed of a 1:1 dyskerin·hTR complex

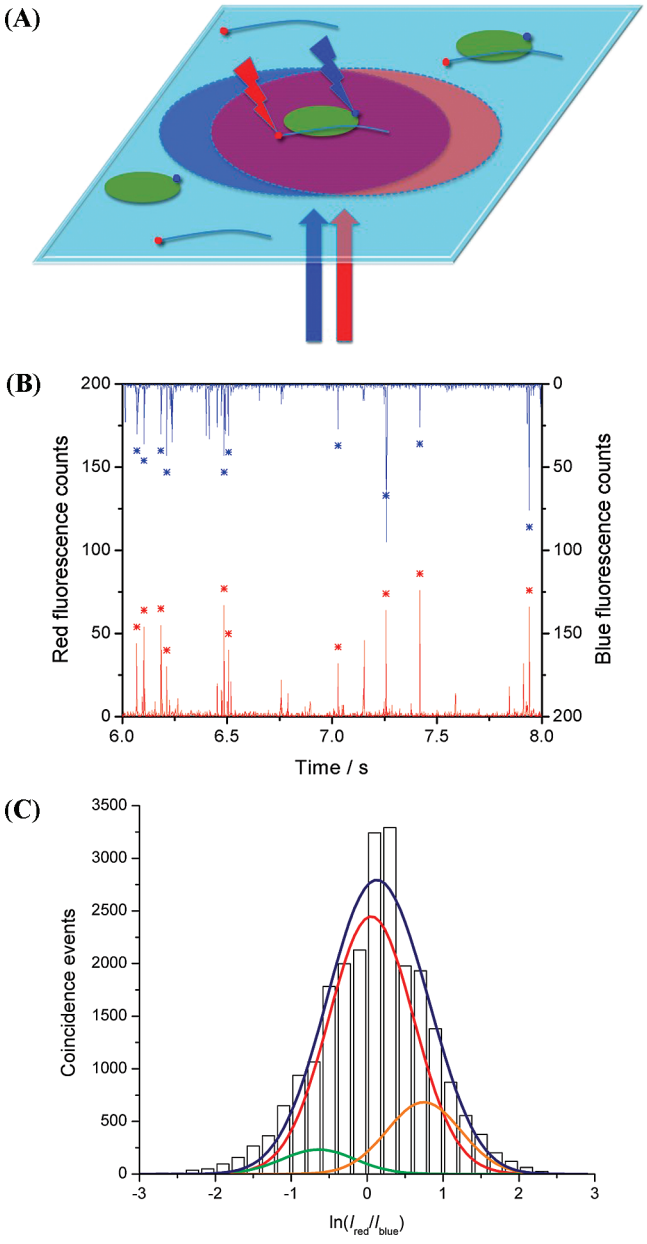


FIGURE 2: (A) Schematic of the single-molecule TCCD system. The green ellipse is a dyskerin molecule and the blue curved line an hTR molecule, and the blue and red filled circles are the fluorophores attached to the two species under investigation. The large light blue and red ellipses represent excitation volumes for the blue and red lasers, respectively, and the large purple ellipse is the overlap volume where both red and blue lasers can simultaneously excite blue and red fluorophores. (B) Example of a TCCD fluorescence trajectory showing traces simultaneously acquired from both red and blue detection channels. Coincidence events, arising from species including both fluorophores, are marked with asterisks. (C) Coincidence histogram of the YFP−dyskerin·647N−hTR sample: total fit, blue; 1:1 dyskerin·hTR complex, red; 1:2 dyskerin·hTR complex, orange; 2:1 dyskerin·hTR complex, green.

(see Figure S1 of the Supporting Information). We have estimated a $K_d$ value of 0.81 ± 0.17 nM for the dyskerin·hTR complex, on the basis of the following assumptions: (a) we corrected for different diffusion times (based on molecular weights), (b) we assumed a 1:1 interaction, (c) we assumed the complex was at equilibrium (no dissociation was observed over 7 h) (see the Supporting Information for a full analysis of the calculation). Our observation that the majority of the dyskerin·hTR complex is 1:1 is consistent with the view that dyskerin contains a single RNA binding domain PUA (*22*), which could interact with either of the two stems present in the 3′ half of hTR. Furthermore, the archael orthologue of dyskerin has been cocrystallized with a single hairpin H/ACA RNA in a 1:1 arrangement (*23*). The presence of a minor (< 20%) 1:2 dyskerin·hTR complex subpopulation is consistent with the ability of hTR to dimerize via a palindromic sequence in loop J7b/8a, which we have previously observed under similar conditions (*24*). The observation of a minor (< 10%) proportion of the 2:1 dyskerin·hTR complex is consistent with the proposal that one copy of each of the four H/ACA RNP proteins can bind to each stem of an H/ACA RNA (*3*).

To characterize more fully the RNA site dependencies of the dyskerin·hTR interaction, we prepared three 5′-end-labeled hTR fragments (Figure 3A) to assess changes in the interaction with dyskerin as measured by changes in TCCD coincidence levels. YFP−dyskerin protein was expressed in the presence of each of the three fragments in turn, and the resulting samples were purified and analyzed by TCCD, as per the wild-type hTR experiments described earlier. The first fragment, 647N−hTR-(353−451), comprised the box H/ACA domain, which consists of a box H consensus sequence (5′-ANANNA-3′) and a box ACA sequence (5′-ACA-3′) on either side of a stem−loop structure at the hTR 3′ end. Previous work using an in vitro reconstitution system has indicated that the hTR box H/ACA domain, specifically nucleotides 379−451, is the sole requirement for assembly of an RNP with the four H/ACA RNP proteins (*25*). In our hands, fragment hTR(353−451) showed a reduction in the fraction of dyskerin·RNA complexes formed to 0.38 ± 0.15, relative to wild-type hTR (Figure 3B). This indicates that the hTR box H/ACA domain alone is not sufficient for full reconstitution of the dyskerin·hTR interaction. The second hTR fragment we studied, 647N−hTR(1−354), was complementary to the first in that it comprised the whole of hTR without the box H/ACA domain. In this case, we observed a reduction in coincidence to 0.72 ± 0.19, which suggests that residues outside the box H/ACA domain are indeed important for proper dyskerin·hTR association. The third hTR fragment, 647N−hTR(1−208), comprised the template/pseudoknot domain alone. This construct demonstrated a reduction in the level of dyskerin·RNA complex formation to 0.29 ± 0.04, which shows that the 5′ half of hTR is capable of an interaction with dyskerin in the absence of both the CR4/CR5 and box H/ACA domains. It is important here to note that in each case we recover similar amounts of dyskerin protein but a smaller fraction of associated complex so that we can directly compare the level of coincidence for each new construct (and later on for mutants) by this method. If the box H/ACA domain were the dominant requirement for dyskerin·hTR interaction, fragments hTR(1−208) and hTR(1−354) would not have exhibited significant complex formation with dyskerin, whereas hTR-(353−451) would have interacted to the same extent as full-length hTR. The data rather indicate that the box H/ACA motif is not the unique dyskerin-binding element within hTR and suggest that binding outside the 3′ terminal 100 nucleotides is also possible.

We next studied the physical consequence of DC-associated mutations in dyskerin and hTR, which have been identified in patients enrolled in a dyskeratosis congenita registry consisting of 328 affected families. In this study, we have chosen three mutations in *DKC1* associated with X-linked DC

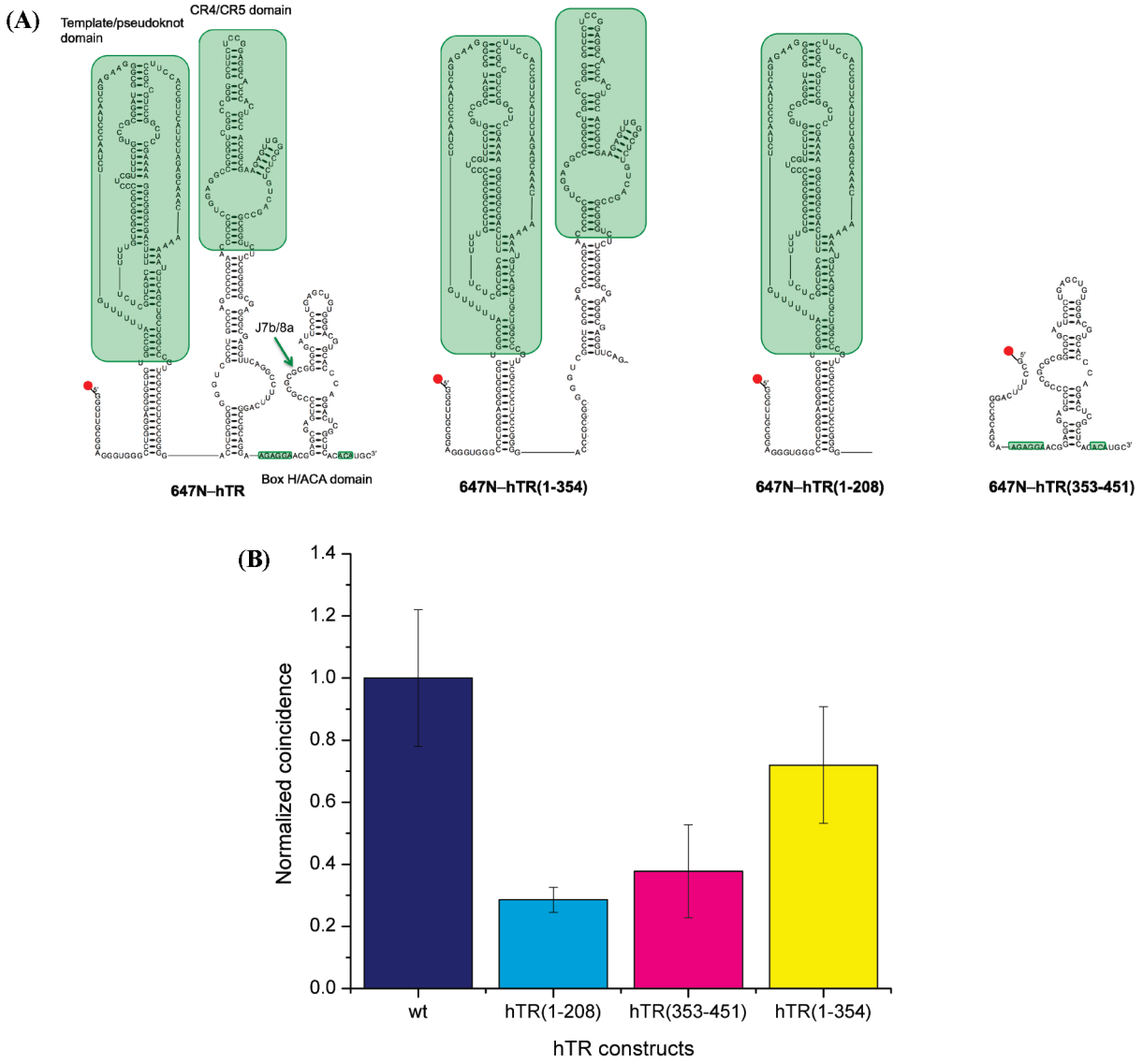


FIGURE 3: (A) Fluorescently labeled wild-type hTR and hTR fragment constructs used in this study. (B) Fraction of complex formed between hTR fragments and wild-type dyskerin, normalized relative to wild-type hTR (dark blue). Values represent averages over at least three independent experiments, and error bars for each fragment are the standard deviation of the normalized mean (except for wild-type hTR, for which error bars represent the standard error of the coincidence values).

to explore whether they affect the interaction with hTR (Figure 4A).

We observed that for each of the DC-associated single-amino acid substitutions in dyskerin that we studied, there was a notable reduction in the fraction of dyskerin·hTR complexes formed (Figure 4B). The coincidence dropped to 0.19 ± 0.03 relative to wild-type dyskerin for the Ala353Val mutation, which is found in 40% of characterized X-linked sufferers and is one of the most prevalent mutations in DC as a whole and a recurrent cause of classical DC as well as some severe phenotypes. A decrease in the normalized coincidence level to 0.39 ± 0.02 was observed for the Gly402Glu mutant, which was found in the first large DC family. The Thr49Met mutation is associated with a severe DC phenotype and has been found in four unrelated cases. This mutation exhibited a smaller but substantial reduction in the fraction of complexes to 0.61 ± 0.02, relative to wild-type dyskerin. Overall, these observations demonstrate that the physical interaction between hTR and dyskerin is disrupted when known dyskerin mutations associated with X-linked DC are employed in our system. Notwithstanding a clear decrease in the fraction of complex formed with the dyskerin mutants, in every case evidence of stoichiometric heterogeneity was detected (see Figure S2A of the Supporting Information). However, in all cases, the dominant contribution remains that of the 1:1 dyskerin·hTR complex.

It has been reported in the literature that patient-derived cells expressing two of these dyskerin mutants (either Ala353Val or Gly402Glu) demonstrated a substantial reduction in hTR levels compared to cells expressing wild-type dyskerin[2] (*20*). In our experiments, mutations Ala353Val and Gly402Glu each caused a substantial reduction in dyskerin·hTR coincidence to below 50% of that of the wild type. The correlation between our biophysical data and the cell biology data reported previously suggests that the dyskerin·hTR interaction is important for the maintenance of appropriate hTR levels in the cell and is consistent with the view that dyskerin binds to hTR to direct proper processing of the primary RNA polymerase II transcript and/or to direct subnuclear localization (*2*, *4*).

[2]There are no in vivo data available yet for the Thr49Met mutant.

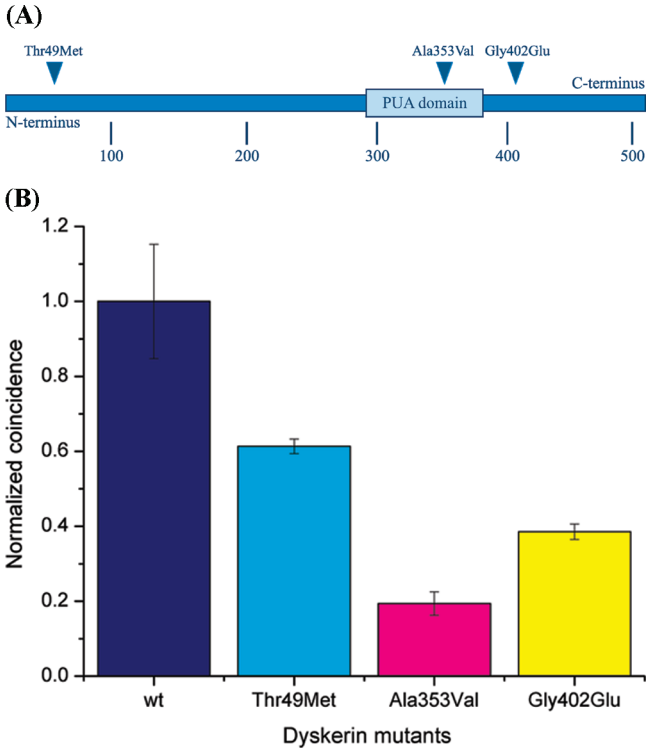


FIGURE 4: (A) Schematic of the *DKC1* protein sequence showing the positions of the three selected dyskerin mutations: Thr49Met, Ala353Val, and Gly402Glu. (B) Fraction of complex formed between dyskerin mutants and wild-type hTR, normalized relative to wild-type dyskerin (dark blue). Values represent averages over at least three independent experiments, and error bars are the standard deviation of the normalized mean (except for wild-type dyskerin, for which error bars represent the standard error of the coincidence values).

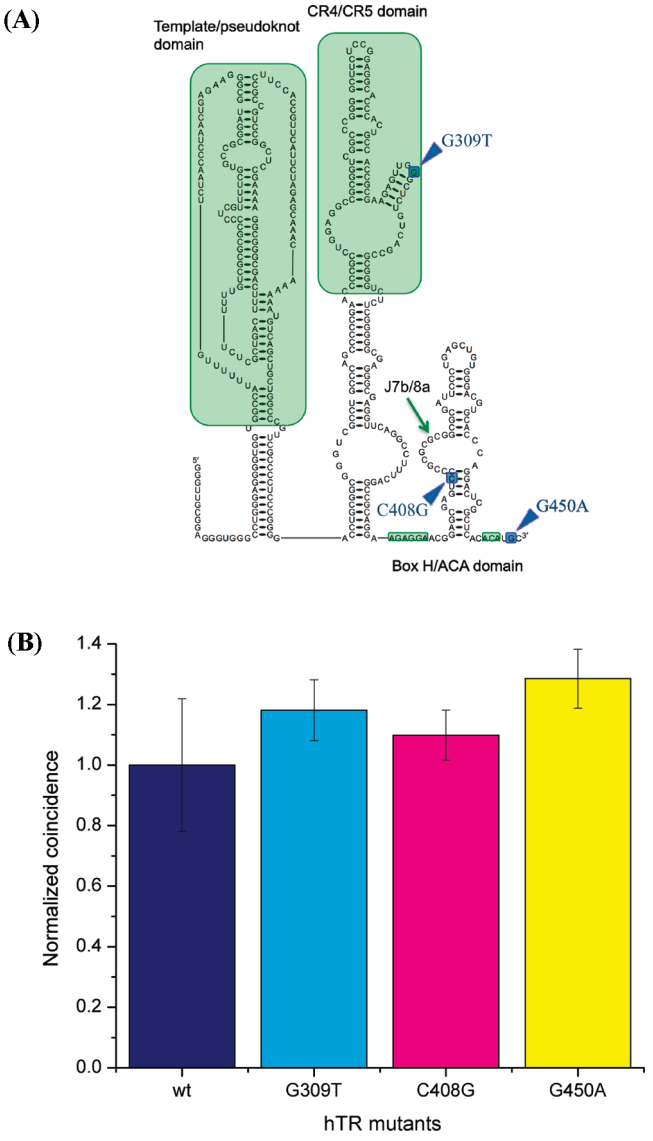


FIGURE 5: (A) Location of the hTR mutations in the 3′ half of the RNA. (B) Fraction of complex formed between hTR mutants and wild-type dyskerin, normalized relative to wild-type hTR (dark blue). Values represent averages over at least three independent experiments, and error bars are the standard deviation of the normalized mean (except for wild-type hTR, for which error bars represent the standard error of the coincidence values).

There are a number of mutations in hTR that are associated with the autosomal dominant form of dyskeratosis congenita. In this part of the study, we set out to probe whether this genetic subtype of the disease is also a consequence of a reduced level of binding between hTR and dyskerin, as we had found in the X-linked form of the disease. The majority of hTR mutations associated with DC are localized in the template/pseudoknot domain, with a smaller number present in the 3′ half of hTR. We elected to investigate three mutations (Figure 5A) that occur in regions of hTR we have now shown to be important for the interaction of hTR with dyskerin, namely, the CR4/CR5 and box H/ACA domains. First, we selected C408G, a mutation found in one of the original DC families with hTR mutations that showed a 75% decrease in levels of observed telomerase catalytic activity (*26*). Second, we selected G450A, found in sporadic cases of DC with normal telomere lengths, which showed catalytic activity indistinguishable from that of wild-type hTR (*27*, *28*). The third mutation, C309T, was chosen as it is located in the CR4/CR5 domain and enabled us to target mutations in two different stem−loop structures found to be important for binding to dyskerin (*29*).

YFP−dyskerin protein was expressed in the presence of the labeled hTR mutants, and the resulting samples were subjected to single-molecule TCCD analysis. We found the fraction of dyskerin·hTR complexes formed for all three hTR mutant complexes to be essentially indistinguishable from the level of the wild-type complex: 1.18 ± 0.10 for G309T, 1.10 ± 0.08 for C408G, and 1.29 ± 0.09 for G450A (Figure 5B). For all three cases studied, we therefore could not link the associated disease phenotype to a decrease in the degree of interaction between dyskerin and hTR, or to changes in the stoichiometry of the interaction (see Figure S2B of the Supporting Information). This suggests that the molecular mechanism leading to suboptimal telomere maintenance may be distinct for the X-linked and autosomal dominant forms of DC for the mutations we have studied.

## CONCLUSIONS

We have provided the first evidence of a direct physical interaction between dyskerin and hTR. Using single-molecule TCCD, we observed dyskerin·hTR complex formation composed mainly of the 1:1 dyskerin·hTR complex, with minor contributions of 1:2 dyskerin·hTR and 2:1 dyskerin·hTR complexes. The higher-order species may arise if hTR is able to dimerize in the presence of dyskerin or if one dyskerin is able to

bind to each of the two hTR box H/ACA stems. By deleting selected domains in hTR, we have shown that the hTR box H/ACA domain alone is not sufficient to promote optimal dyskerin·hTR binding, and that in fact dyskerin is able to bind to other regions of hTR outside the 3′ terminal 100 nucleotides.

We have related the dyskerin·hTR interaction to human disease by evaluating dyskerin mutations associated with the X-linked form of dyskeratosis congenita. Our study revealed a significant impairment in formation of the dyskerin·hTR complex for each mutant dyskerin. The first mutation, Ala353-Val, is in the so-called pseudouridine and archaeosine transglycosylase (PUA) domain, which has been proposed as an RNA binding domain, by analogy with the archael and *Escherichia coli* homologues, Cbf5 and TruB, respectively. According to a predicted folded structure of dyskerin, based on the structure of the archael Cbf5, the other two mutations result in amino acid changes close in space to the PUA domain (*22*). The observed decrease in coincidence, for each of the dyskerin mutants, supports a telomerase biogenesis mechanism in which dyskerin·hTR RNP complex formation is important. Efficient dyskerin·hTR RNP complex formation may be a necessity for normal hTR levels within the cell, pointing to a role for dyskerin at an early stage of telomerase biogenesis prior to hTERT binding. Thus, we propose that mutations in dyskerin may lead directly to X-linked DC by disruption of the dyskerin·hTR interaction. In contrast, we observed no change in dyskerin·hTR complex formation for the autosomal dominant DC hTR mutants we studied [G309T, C408G, and G450A (Figure 5A)], suggesting that such mutations probably act via a distinct mechanism at the molecular level.

The single-molecule TCCD approach has enabled the biophysical exploration of an important biomolecular interaction that was, in our hands, inaccessible by classical physical methods. The data have provided insights into what might contribute to the molecular basis of clinically relevant mutations, which may inspire a consideration of therapeutics that compensate for the effects of these mutants and restore normal dyskerin·hTR interaction and proper functioning of the system.

## SUPPORTING INFORMATION AVAILABLE

Data to support the observed stoichiometry of the YFP−dyskerin·647N−hTR complex where both wild-type and mutated components are detailed. This material is available free of charge via the Internet at http://pubs.acs.org.

## REFERENCES


1. Hamma, T., and Ferré-D'Amaré, A. (2006) Pseudouridine synthases. *Chem. Biol. 13*, 1125–1135.
2. Mitchell, J., Cheng, J., and Collins, K. (1999) A box H/ACA small nucleolar RNA-like domain at the human telomerase RNA 3′ end. *Mol. Cell. Biol. 19*, 567–576.
3. Meier, U. (2005) The many facets of H/ACA ribonucleoproteins. *Chromosoma 114*, 1–14.
4. Mitchell, J., Wood, E., and Collins, K. (1999) A telomerase component is defective in the human disease dyskeratosis congenita. *Nature 402*, 551–555.
5. Theimer, C., and Feigon, J. (2006) Structure and function of telomerase RNA. *Curr. Opin. Struct. Biol. 16*, 307–318.
6. Cohen, S., Graham, M., Lovrecz, G., Bache, N., Robinson, P., and Reddel, R. (2007) Protein composition of catalytically active human telomerase from immortal cells. *Science 315*, 1850–1853.
7. Fu, D., and Collins, K. (2007) Purification of human telomerase complexes identifies factors involved in telomerase biogenesis and telomere length regulation. *Mol. Cell 28*, 773–785.
8. Vulliamy, T., and Dokal, I. (2008) Dyskeratosis congenita: The diverse clinical presentation of mutations in the telomerase complex. *Biochimie 90*, 122–130.
9. Kirwan, M., and Dokal, I. (2008) Dyskeratosis congenita: A genetic disorder of many faces. *Clin. Genet. 73*, 103–112.
10. Zinsser, F. (1906) Atophia cutis reticularis cum pigmentatione dystophia unguium et leukoplakia oris, pp 219−223, Ikonogr. Dermatol. (Hyoto).
11. Wong, J., and Collins, K. (2003) Telomere maintenance and disease. *Lancet 362*, 983–988.
12. Heiss, N., Knight, S., Vulliamy, T., Klauck, S., Wiemann, S., Mason, P., Poustka, A., and Dokal, I. (1998) X-linked dyskeratosis congenita is caused by mutations in a highly conserved gene with putative nucleolar functions. *Nat. Genet. 19*, 32–38.
13. Knight, S., Heiss, N., Vulliamy, T., Greschner, S., Stavrides, G., Pai, G., Lestringant, G., Varma, N., Mason, P., Dokal, I., and Poustka, A. (1999) X-linked dyskeratosis congenita is predominantly caused by missense mutations in the DKC1 gene. *Am. J. Hum. Genet. 65*, 50–58.
14. Dokal, I., and Vulliamy, T. (2003) Dyskeratosis congenita: Its link to telomerase and aplastic anaemia. *Blood Rev. 17*, 217–225.
15. Vulliamy, T., Marrone, A., Goldman, F., Dearlove, A., Bessler, M., Mason, P., and Dokal, I. (2001) The RNA component of telomerase is mutated in autosomal dominant dyskeratosis congenita. *Nature 413*, 432–435.
16. Li, H., Ying, L., Green, J., Balasubramanian, S., and Klenerman, D. (2003) Ultrasensitive coincidence fluorescence detection of single DNA molecules. *Anal. Chem. 75*, 1664–1670.
17. Orte, A., Clarke, R., Balasubramanian, S., and Klenerman, D. (2006) Determination of the fraction and stoichiometry of femtomolar levels of biomolecular complexes in an excess of monomer using single-molecule, two-color coincidence detection. *Anal. Chem. 78*, 7707–7715.
18. Clarke, R., Orte, A., and Klenerman, D. (2007) Optimized threshold selection for single-molecule two-color fluorescence coincidence spectroscopy. *Anal. Chem. 79*, 2771–2777.
19. Kim, N., Piatyszek, M., Prowse, K., Harley, C., West, M., Ho, P., Coviello, G., Wright, W., Weinrich, S., and Shay, J. (1994) Specific association of human telomerase activity with immortal cells and cancer. *Science 266*, 2011–2015.
20. Walne, A., Vulliamy, T., Marrone, A., Beswick, R., Kirwan, M., Masunari, Y., Al-Qurashi, F., Aljurf, M., and Dokal, I. (2007) Genetic heterogeneity in autosomal recessive dyskeratosis congenita with one subtype due to mutations in the telomerase-associated protein NOP10. *Hum. Mol. Genet. 16*, 1619–1629.
21. Alves, D., Li, H., Codrington, R., Orte, A., Ren, X., Klenerman, D., and Balasubramanian, S. (2008) Single-molecule analysis of human telomerase monomer. *Nat. Chem. Biol. 4*, 287–289.
22. Rashid, R., Liang, B., Baker, D., Youssef, O., He, Y., Phipps, K., Terns, R., Terns, M., and Li, H. (2006) Crystal structure of a Cbf5-Nop10-Gar1 complex and implications in RNA-guided pseudouridylation and dyskeratosis congenita. *Mol. Cell 21*, 249–260.
23. Li, L., and Ye, K. (2006) Crystal structure of an H/ACA box ribonucleoprotein particle. *Nature 443*, 302–307.
24. Ren, X., Gavory, G., Li, H., Ying, L., Klenerman, D., and Balasubramanian, S. (2003) Identification of a new RNA·RNA interaction site for human telomerase RNA (hTR): Structural implications for hTR accumulation and a dyskeratosis congenita point mutation. *Nucleic Acids Res. 31*, 6509–6515.
25. Dragon, F., Pogacić, V., and Filipowicz, W. (2000) In vitro assembly of human H/ACA small nucleolar RNPs reveals unique features of U17 and telomerase RNAs. *Mol. Cell. Biol. 20*, 3037–3048.
26. Marrone, A., Stevens, D., Vulliamy, T., Dokal, I., and Mason, P. (2004) Heterozygous telomerase RNA mutations found in dyskeratosis congenita and aplastic anemia reduce telomerase activity via haploinsufficiency. *Blood 104*, 3936–3942.
27. Ly, H., Calado, R., Allard, P., Baerlocher, G., Lansdorp, P., Young, N., and Parslow, T. (2005) Functional characterization of telomerase RNA variants found in patients with hematologic disorders. *Blood 105*, 2332–2339.
28. Vulliamy, T., Walne, A., Baskaradas, A., Mason, P., Marrone, A., and Dokal, I. (2005) Mutations in the reverse transcriptase component of telomerase (TERT) in patients with bone marrow failure. *Blood Cells, Mol., Dis. 34*, 257–263.
29. Kirwan, M., Vulliamy, T., Marrone, A., Walne, A., Beswick, R., Hillmen, P., Kelly, R., Stewart, A., Bowen, D., Schonland, S., Whittle, A., McVerry, A., Gilleece, M., and Dokal, I. (2009) Defining the pathogenic role of telomerase mutations in myelodysplastic syndrome and acute myeloid leukemia. *Hum. Mutat. 30*, 1–7.